scientific reports

Check for updates

OPEN

Synthesis of lignin-derived nitrogen-doped carbon as a novel catalyst for 4-NP reduction evaluation

Yun Liu[1,2,3,4]✉, Huanghui Xu[1], Hongfei Yu[1], Haihua Yang[1] & Tao Chen[2,3,4]

In this study, nitrogen-doped carbon (NC) was fabricated using lignin as carbon source and g-C_3N_4 as sacrificial template and nitrogen source. The structural properties of as-prepared NC were characterized by TEM, XRD, FT-IR, Raman, XPS and BET techniques. Attractively, NC has proved efficient for reducing 4-nitrophenol (4-NP) to 4-aminophenol (4-AP) using $NaBH_4$ as hydrogen donor with high apparent rate constant (k_{app} = 4.77 min^{-1}) and specific mass activity (s = 361 mol $kgcat^{-1}$ h^{-1}), which values are superior to the previously reported catalysts in the literature. Density functional theory (DFT) calculations demonstrate that four kinds of N dopants can change the electronic structure of the adjacent carbon atoms and contribute to their catalytic properties dependant on N species, however, graphitic N species has much greater contribution to 4-NP adsorption and catalytic reduction. Furthermore, The preliminary mechanism of this transfer hydrogenation reaction over as-prepared NC is proposed on the basis of XPS and DFT data. Astoundingly, NC has excellent stability and reusability of six consecutive runs without loss of catalytic activity. These findings open up a vista to engineer lignin-derived NC as metal-free catalyst for hydrogenation reaction.

Lignin, the second-most abundant renewable aromatic biopolymer in nature, accounts for 15–30 wt% of lignocellulosic biomass. It has been taking hold of the scientific community agenda in the biomass biorefinery[1–3]. Depolymerization through oxidation and/or reduction strategies into monomeric, aromatic compounds is the current prevalent method of lignin valorisation[4–6]. In 2014, Rahimi et al. described a method for the depolymerization of oxidized lignin under mild conditions in aqueous formic acid that resulted in more than 60 wt% yield of low-molecular-mass aromatics[7]. In 2018, Wu et al. reported an electron–hole coupled photoredox mechanism to cleavage β-O-4 bond in lignin with the yield of about 27 wt% of aromatic monomers from birch woodmeal[8]. Besides efforts in the depolymerization of lignin towards low-molecular-mass aromatics, attempts to convert this polymer into lignin-derived carbon-based catalysts have been recently reported[9–11]. For instance, in 2019, Zhou et al. developed the assembly of lignin–metal complexes for producing bimetallic nanoparticles catalyst and/or metal single-atom catalysts supported on nitrogen-doped carbon using lignin as covalent ligand, which opens new avenue towards lignin-derived functional catalytic materials[10,11].

In comparison with metallic catalysts, metal-free catalysts like carbon materials have many outstanding merits of low-cost, bio-degradation, environmental friendly and readily available aspects, which can avoid heavy metals environmental pollution and depletion of rare metal resources[12–15]. Heteroatomic dopants, e.g. S-, B-, P- and N-doped carbon materials can change electronic density structure of the adjacent carbon atoms and promote their catalytic activities, they have been successfully applied in electrochemical reaction[16], supercapacitor electrodes[17], catalytic oxidation[18], and reduction reaction[19]. For instance, Lin et al. described a boron-doped carbon material that showed excellent chemoselective reduction ability of nitroarenes with good conversions (99%) for substrates and selectivities (88%) for desired products[20]. Duan et al. synthesized a N,P-codoped carbon exhibiting excellent activity and exclusive selectivity for catalytic transfer hydrogenation of nitroarenes[21]. More recently, N-doped reduced graphene oxide (NG) has been found to be an effective metal-free catalyst for 4-NP

[1]College of Life Science and Technology, Beijing University of Chemical Technology, Beijing 100029, China. [2]School of Nuclear Technology and Chemistry and Biology, Hubei University of Science and Technology, Xianning 437100, China. [3]Hubei Key Laboratory of Radiation Chemistry and Functional Materials, Hubei University of Science and Technology, Xianning 437100, China. [4]Hubei Engineering Research Center for Fragrant Plants, Hubei University of Science and Technology, Xianning 437100, China. ✉email: liuyun@mail.buct.edu.cn

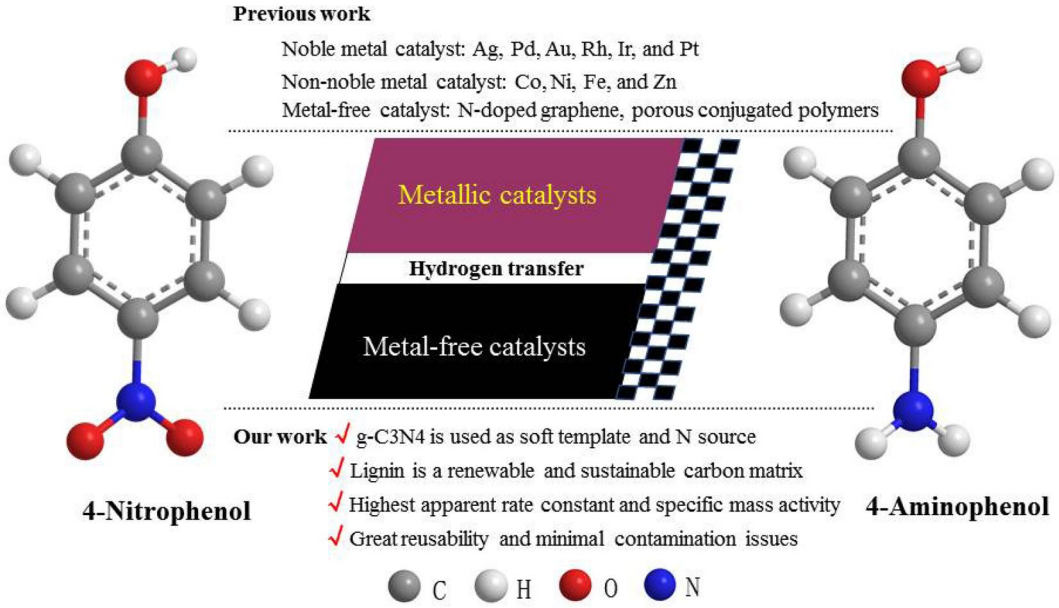

Scheme 1. Overviews of 4-nitrophenol (4-NP) reduction to 4-aminophenol (4-AP) through hydrogenation reaction by different catalysts in previous and our works.

reduction, a key transformation in fine chemical synthesis[19,21–23]. In the last decades, extensive investigations on this reaction have been conducted over both metallic catalysts[22,24–26] and metal-free catalysts[12,19,20,23,27].

In the present work, a lignin-derived N-doped carbon (NC) was synthsized through evaporation-induced deposition approach followed by carbonization treatment. It could be used as efficient metal-free catalyst for the conversion of 4-nitrophenol (4-NP) to 4-aminophenol (4-AP) with $NaBH_4$ as hydrogen donor. To our best knowledge, no studies have been yet reported to synthesize NC using lignin as carbon source and g-C_3N_4 as soft template and N source, which has a high N content (57.1%) and complete decomposition at temperature above 710 °C[28]. In our work, the main objectives are to investigate the effect of lignin/g-C_3N_4 mass weight ratio and annealing temperature on the structure and activity of the desired NC catalysts. Furthermore, density function theory (DFT) is employed to address two critical issues for 4-NP reduction over the as-prepared NC. One is to state the preferred binding sites related to nitro group and/or the O atom of hydroxyl substitutes. The other is to examine the contributions of four kinds of nitrogen dopants to catalytic activity. In addition, the reaction kinetics and stability of the as-prepared NC are evulated for 4-NP reduction. According to experimental data and DFT calculations, a plausible catalytic mechanism of 4-NP over this desired NC catalyst is proposed. These findings in our work will pave a new avenue about lignin valorisation towards nitrogen-doped carbon-based catalyst for hydrogenation reaction.

As shown in Scheme 1, compared with the earlier reported articles, several outstanding merits will be found in this present work, (1) g-C_3N_4 with high surface specific area (S_{BET} = 1200 m^2/g) and high N content (57.1%) is used as sacrificial template (decomposition at 710 °C) and N source; (2) low-cost abundant lignin is employed as a renewable carbon matrix; (3) the as-prepared NC catalyst with high apparent rate and mass specific activities for 4-NP reduction outperforms most of the previous reported catalysts in the literature; (4) the as-prepared NC catalyst shows excellent re-usability and causes no environmental contamination issues through catalyst recycling.

Materials and methods

Lignin isolated from *Eucalyptus* biomass using aqueous formic acid (FA) fractionation. Lignin was isolated from eucalyptus wood using formic acid aqueous solution according to the modified procedures detailed in the literature[29], and the FA fractionation procedure was shown in Supplementary Fig. S1. Briefly, 445 mL FA with the concentration of 70% was filled in 2 L round-bottom glass flask, which was loaded with 44 g *Eucalyptus* powder. The solid mass weight (g) to liquid volume (mL) ratio was set at approx. 1:100. The mixture was stirring at 1300 rpm and 130 °C for 3 h. After the desired reaction time, the mixture was filtered. The black liquor filtrate was collected and evaporated in vacuum condition to recover FA. After FA recovery, lignin was precipitated at the bottom of the flask. The precipitated lignin was washed with 300 mL distilled water and then filtered to separate lignin from aqueous phase. After dried, approx. 9 g of lignin pellets were obtained. According to the method detailed in our previous work[30], the compositions of the obtained lignin were calculated to be 90.31% of lignin with small amount of cellulose (0.8%), hemicellulose (0.24%) and others (2.43%). The morphology of lignin show sphere appearance and the particle size of lignin nanoparticle is approx. 83 nm (Supplementary Fig. S1).

g-C_3N_4 soft temple preparation. g-C_3N_4 was prepared by high-thermal decomposition polymerization of urea[31]. Typically, 28 g of urea was transferred to 50 mL lidded porcelain crucible, and then heated in a muffle furnace from room temperature to 550 °C at the heating rate of 2 °C min^{-1} and kept at 550 °C for 4 h. After cooling to room temperature, about 1.81 g of g-C_3N_4 was obtained in our work. The surface specific area (S_{BET}) of the obtained g-C_3N_4 sample was measured to be 1200 m^2/g) and its total N content was 57.1%.

Lignin-derived nitrogen-doped carbon (NC) catalyst synthesis through evaporation-induced deposition approach followed with carbonization treatment. The synthesis procedure of evaporation-induced deposition approach was conducted to prepare lignin-derived nitrogen-doped carbon (NC) catalyst. Typically, the amount of g-C_3N_4 was dispersed in 100 mL of 70% FA aqueous solution, in which 1 g lignin with the final concentration of 1 wt% was dissolved under ultrasonic condition for 30 min. The mass weight ratio of g-C_3N_4 to lignin was set at 2, 6, 10, 14 and 18. The FA in the resulting suspension was evaporated at 45 °C under vacuum condition and lignin nanoparticles were homogeneously deposited onto the surface of g-C_3N_4. Afterwards, five samples (g-C_3N_4@lignin) dependant on the mass ratio of g-C_3N_4/lignin were collected and dried in an oven at 80 °C overnight. Five g-C_3N_4@lignin products were milled in agate mortar for approx. 45 min. About 3 g of powder was tiled in porcelain boat and calcined at 1073 K, 1173 K, 1273 K and 1373 K, respectively for 2 h in an argon atmosphere to yield a score of N_xC-T catalysts (x represents the N content (x = 2, 6, 10, 14 and 18), T = 1073 K, 1173 K, 1273 K and 1373 K, respectively). The experimental design of N_xC-T catalysts syntheses was shown in Supplementary Fig. S2. As a control, sole lignin without g-C_3N_4 template was annealed at 1373 K for 2 h in an argon atmosphere, it was labeled as LC-1373.

Structural properties characterization of N_xC-T catalysts. The morphology of transmission electronic microscope (TEM) image was collected on a Hitachi H-800 spectroscope (Japan) operating at 10 kV. Fourier Transform infrared spectroscopy (FT-IR) profiles were recorded on a Bruker Vertex 70 (German) from 400 to 4000 cm^{-1} at a resolution of 2 cm^{-1}, equipped with a temperature- controlled attenuated total reflectance (ATR) device with a ZnSe crystal (Pike Technology). X-ray photoelectron spectroscopy (XPS) was performed on a ThermoFisher Scientific ESCALAB 250XI (USA) using monochromated Al Kalph source (150 W, 500 μm). The pass energy was 50 eV for survey, and 30 eV for high resolution scans. All binding energies were reference to the C1s peak at 284.4 eV. X-ray diffraction (XRD) patterns were recorded on a Bruker D2-phaser diffractometer (German) at 40 mA and 40 kV using Cu Kα radiation (λ = 1.54, 6.88°/min from 5 to 90°). Raman spectra were recorded on a Renishaw inVia Micro-Raman Spectroscopy System (England) equipped with charge-coupled device detector at 633 nm. Specific surface areas and pore size distributions were determined by Brunauer Emmett-Teller (BET) method on Micromeritics ASAP 2460 apparatus (USA) from nitrogen sorption isotherms collected at 77 K. The samples were degassed at 250 °C for 12 h prior to measurement.

Catalytic performance of 4-NP reduction over NxC-T catalysts. 140.5 mg of 4-NP was dissolved in 100 mL deionized water using as stock solution and kept in a brown bottle at 4 °C for use. Then, 5 mg of NC catalysts were homogeneously dispersed in 200 mL of deionized water under ultrasonic condition for 5 min and immersed into water bath at 25 °C under stirring condition for 10 min. Subsequently, 1.6 mL of 4-NP and 6.4 mmol of $NaBH_4$ were added into the solution. After a certain regular time interval, an aliquot of 4 mL was taken from the reaction mixture. The NC catalyst was separated by filtering via 0.22 μm membrane, and the obtained transparent solution was used for absorption spectral analysis by UV756 UV–visible spectrophotometer (Shanghai, China).

Reaction kinetics of 4-NP reduction over NC catalyst was investigated using $NaBH_4$ as hydrogen donor in water. Pseudo-first-order kinetics model was applied in our work because $NaBH_4$ was greatly excessive and its concentration was regarded as being constant in the reaction[32]. Therefore, the apparent rate constant (k_{app}) was calculated by Eq. (1):

$$-k_{app}t = \ln \frac{C_t}{C_0} \tag{1}$$

where C_0 and C_t was the concentration of 4-NP at initial and assigned reaction time (t), respectively. The value of k_{app} could be calculated from the slope of the fitting line $\ln \frac{C_t}{C_0} \rightarrow t$.

To assess the catalytic activity of the as-synthesized NC catalyst in our work, specific mass activity was evaluated according to Eq. (2):

$$Specific\ mass\ activity = \frac{N}{M_{cat}T} \tag{2}$$

where N means the mole fraction of 4-NP at assigned reaction time, mol; M_{cat} is the mass weight of catalyst, kg; T represents the reaction time, h.

To investigate the effect of nitrogen dopant on the activity of lignin-derived NC catalysts, several counterparts including LC-1373, graphite powder, g-C_3N_4, graphene oxide (GO), and N_{14}C-1373 were compared for the conversion of 4-NP to 4-AP. The catalysts LC-1373, g-C_3N_4 and N_{14}C-1373 were synthesized in our lab, while graphite powder and GO were bought from Beijing local reagent company.

The recycling experiments of as-prepared NC catalyst were also examined for six runs. For each trial, the used catalyst was separated and washed with deionized water three times before next batch. Each reaction trial was run in triplicates and the average value was used as the final result in this work. For comparison, commercial

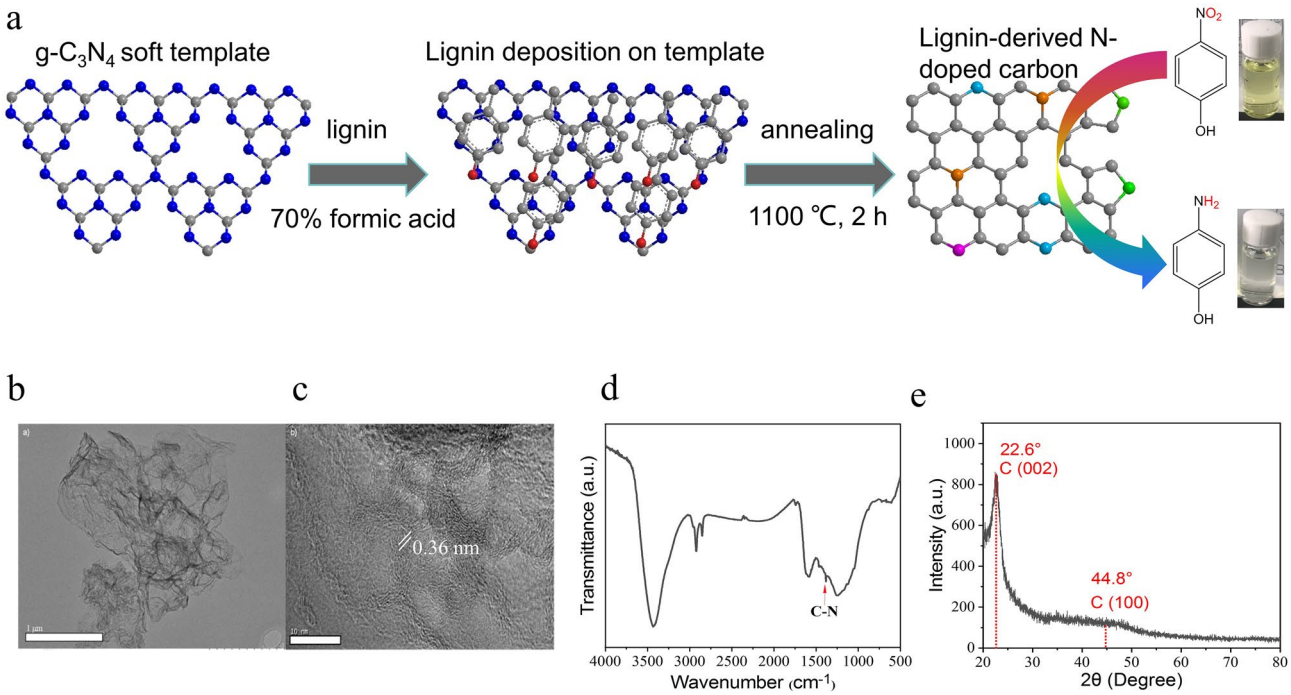

Figure 1. Lignin-derived NC synthesis and its structural properties. (**a**) Schematic overview for the synthesis procedure of lignin-derived NC at 1100 °C for 2 h. Lignin was dissovled in FA solution. After FA evaporation, lignin with sphere appearance and the particle size of approx. 83 nm was deposited on the surface of g-C_3N_4 template. (**b**) TEM image of N_{14}C-1373. (**c**) HR-TEM image of N_{14}C-1373. (**d**) FT-IR profile of N_{14}C-1373. (**e**) XRD pattern of N_{14}C-1373.

Pb/C catalyst was employed in the 4-NP catalytic test under the same conditions to assess metallic catalytic activity and metal leaching.

Density functional theory (DFT) calculation. To address the preferred binding sites of 4-NP over NC catalyst and nitrogen dopants contribution of NC catalyst to the catalytic performance, DFT simulations were performed by Vienna ab-initio simulation package (VASP) with the projector augmented wave pseudo-potentials (PAW) to describe the interaction between atomic cores and valence electrons[33]. The Perdew–Burke–Ernzerhof (PBE) function within the generalized gradient approximation (GGA) was used to implement DFT calculations. The N-doped graphene cluster models (20 Å × 20 Å × 12 Å) were employed to simulate the surface properties. The reasonable vacuum layers were set around 12 Å in the z-directions for avoiding interaction between planes. A cutoff energy of 400 eV was provided, and a 2 × 2 × 1 Monkhorst Pack k-point sampling was chosen for the well converged energy values. The optimum geometry structure of NC catalyst was pursued until the force on each atom fell below the convergence criterion of 0.02 eV/Å, and energies were converged within 10^{-5} eV[34,35].

Results and discussion

Synthesis of lignin-derived NC catalyst and its structural characterization. The synthesis procedure of lignin-derived NC was shown in Fig. 1a using lignin as carbon source and g-C_3N_4 as both nitrogen source and sacrificial template. The synthesis procedure was mainly divided into two steps, lignin deposition on template surface and calcination. In brief, g-C_3N_4 template was homogeneously dispersed in 70% FA solution, in which 1% lignin was dissolved. The mass weight ratio of g-C_3N_4 to lignin was set at 2, 6, 10, 14 and 18. After FA evaporation, lignin nanoparticles were deposited on the surface of template. Subsequently, the lignin/g-C_3N_4 was annealled at the assigned temperature for 2 h. Then 20 kinds of N_xC-T catalysts were obtained in dependence of annealing temperature and N content (Supplementary Fig. S2; Supplementary Table S1). In our work, lignin was chosen as carbon source due to its abundance in carbon content (~ 60 to 70 wt%), sustainability and low-cost because lignin has been typically viewed as byproduct of biomass refinery[36]. While g-C_3N_4 was chosen as both template and N source due to its nitrogen-rich (57.1 at%), 3D pore structure and complete decomposition at above 700 °C[31]. To the bset of our knowledge, few articles have yet been available utilizing lignin as carbon source and g-C_3N_4 as both template and nitrogen source to fabricate NC catalyst. To our delight, the as-synthesized NC showed high catalytic activity for 4-NP reduction and outperformed most of the previously reported catalysts in the literature[19–27].

Using N_{14}C-1373 as an example, the morphology of the resultant NC was characterized by TEM. As shown in Fig. 1b, the NC sample is wrinkle veil-like thin nanosheet. It is the consequence of thermal reduction and exfoliation[19]. The high-resolution TEM image (Fig. 1c) further confirms that the nanosheet consists of 3–10 layers. The average distance of interlayer is 0.36 nm, similar to the interlayer distance of graphite (~ 0.34 nm). It

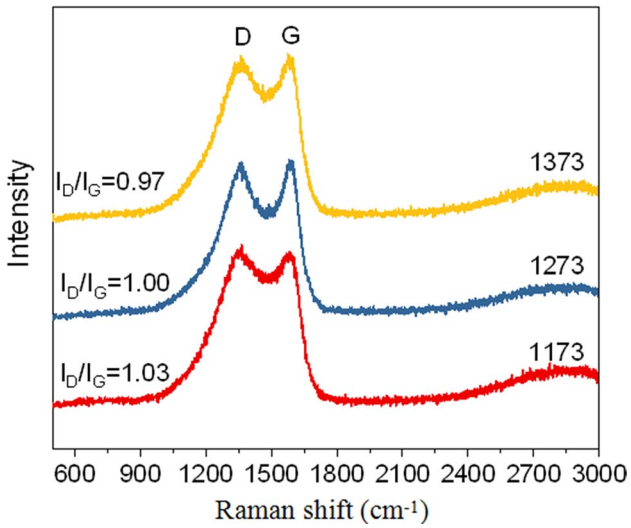

Figure 2. Raman spectra of $N_{14}C$ at different annealing temperatures of 1173, 1273 and 1373 K. The I_D/I_G values represent the graphitizable degree of carbon material. The lower of the I_D/I_G value, the higher of graphitizable degree of carbon material.

is indicating that lignin is graphitizable at high annealing temperature of 1373 K. This phenomenon was demonstrated in our previous work, in which it was found that lignin started to graphitize at 600 °C and graphitizable carbon could be obtained at 1000 °C[10,11]. The FT-IR peak in Fig. 1d at approx. 1380 nm^{-1} is ascribed to C-N stretch, showing N atom is successfully doped into graphitizable carbon[27], although the peak at 1380 cm^{-1} is weak. Further insight into the micro-structure of NC from XRD pattern (Fig. 1e), two peaks at 22.6° and 44.8° are observed, which is ascribed to (002) and (100) planes of graphite-like structure[12,37], respectively. It indicates that the well-ordered graphene with 0.34 nm space is obtained after annealing process[19].

The influence of annealing temperature (1173 K, 1273 K and 1373 K) on the graphitizable degree of $N_{14}C$ was characterized by Raman spectra and shown in Fig. 2. As seen in Raman spectra profiles, peak at 1344 cm^{-1} assigned to disordered sp^3 carbon (D band) and peak at 1599 cm^{-1} ascribed to graphitic sp^2 carbon (G band) are observed. The I_D/I_G values of $N_{14}C$-1173, $N_{14}C$-1273, $N_{14}C$-1373 are 1.03, 1.00, and 0.97, respectively. It indicates that graphitizable degree of $N_{14}C$ increases with the increasing of the calcination temperature. The phenomenon is good consistence with the result reported in our previous work[10,11]. However, it is different from the phenomenon described by Yang et al., who pointed out that I_D/I_G value of nitrogen-doped graphene (NG) decreased as the increasing temperature due to NG partially reduced at high temperature[19].

To address the effect of g-C_3N_4/lignin ratio and annealing temperature on the elemental composition and N species of NC catalysts, XPS measurement was conducted and the results are shown in Fig. 3. The relative atom ratios of C, N and O element of NC samples are summarized in Supplementary Table S2.

Figure 3a shows the effect of annealing temperature on the types of N species of NC. The high resolution N1s XPS spectra can be deconvolved into four types of N species, namely, pyridinic N at 398.6 eV, pyrrolic N at 399.2 eV, graphite N at 400.5 eV and pyridinic N oxide at 402.6 eV, respectively[19,27]. The atomic concentration of total N in each sample is ranging from 3.3 at% to 14.8 at% (Fig. 3c). With an increase annealing temperature from 1073 to 1373 K, the content of total N in each sample decreases (Supplementary Table S2). It is probably ascribed to low thermal stability of nitrogen species at high temperature[19]. However, the graphite N species content in $N_{14}C$-1073, $N_{14}C$-1173, $N_{14}C$-1273, and $N_{14}C$-1373 is calculated to be 26 at%, 45 at%, 52 at% and 69 at%, respectively. Therefore, the ratios of the graphite N to the total N content increase with the enhancement of annealing temperature. The reasonable explanation is the fact that the graphite N species is thermo-stable and the total N content decreases due to other N species directly removing from the graphene sheet[19]. The variance of graphite N species in dependence of temperature is good consistence with the tendency of I_D/I_G calculated from Raman spectra (Fig. 2).

Figure 3b shows the XPS spectra of NC in dependence of g-C_3N_4/lignin ratio at the same annealing temperature of 1373 K. It is worthly noticed that the amount of g-C_3N_4 has little influence on the N content (Fig. 3d). It is probably due to decomposition of g-C_3N_4 at high temperature, resulting in limited N-doped sites in graphitization carbon surface. This phenomenon is also confirmed by FT-IR detection in Fig. 1d. The XPS result (Supplementary Table S2) related to different g-C_3N_4/lignin ratio indicates a 27–31:1 ratio between C and N content.

Annealing temperature has significant effect on the specific surface area and pore diameter size of NC catalysts, which was determined by BET measurement using $N_{14}C$-T as an example (Fig. 4). In absence of g-C_3N_4 template, the N_2 adsorption isotherms for LC-1373 shows a type I curve (Fig. 4a). On the contrary, using g-C_3N_4 as soft template, the N_2 adsorption isotherms for NC samples show a type IV curve with a hysterias loop (Fig. 4b–d), indicating both micro- and mesoporosity[38]. In comparison with LC-1373 (without g-C_3N_4 template, S_{BET} = 402.3 m^2/g), the BET specific surface areas (S_{BET}) determined for $N_{14}C$-1173, $N_{14}C$-1273 and $N_{14}C$-1373 are 626.2 m^2/g, 668.6 m^2/g and 1481.9 m^2/g, respectively. Their corresponding pore sizes were 19.5, 18.1, and 17.1 nm,

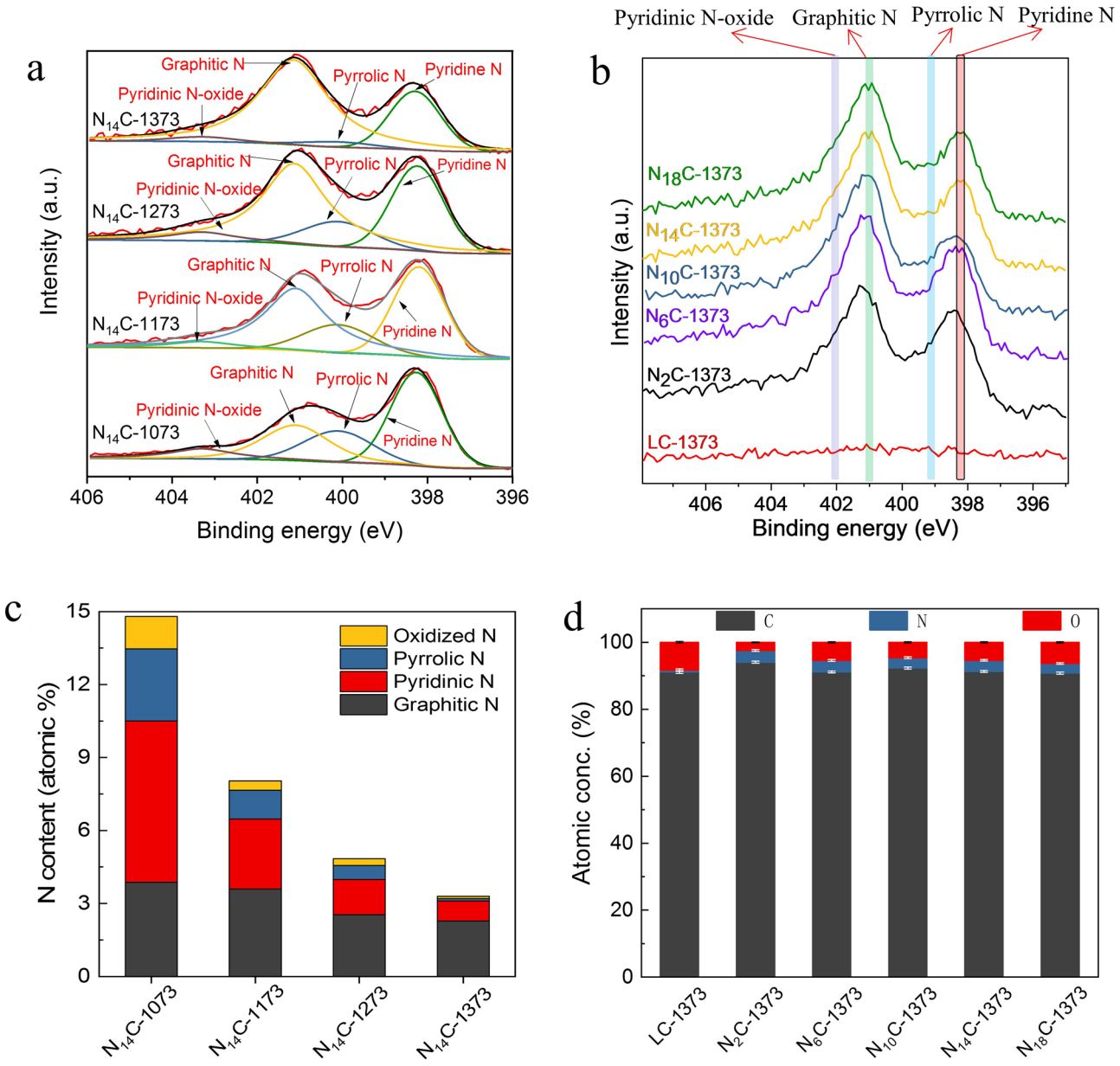

Figure 3. XPS spectra of NC at different annealing temperature and g-C_3N_4/lignin ratio. (**a**) N 1 s scans of NC at different temperature. (**b**) XPS spectra of NC at different g-C_3N_4/lignin ratio. (**c**) Nitrogen content of each type of N species at different temperature. (**d**) Element content of NC samples at different g-C_3N_4/lignin ratio.

respectively. It is evident that g-C_3N_4 serving as template is highly beneficial to achieving high S_{BET} of NC and additional mesoporosity into the samples[39]. In combination with the data in Raman spectra (Fig. 2), a reasonable conclusion has been drawn that the formation of ordered graphite-like layers is contribution to achieving high S_{BET} of the NC. For instance, N_{14}C-1373 has the lowest value of I_D/I_G (=0.97) relative to N_{14}C-1173 (I_D/I_G = 1.03) and N_{14}C-1273 (I_D/I_G = 1.00), it shows the maximal S_{BET} (1481.9 m^2/g). The structural change of carbon material occurring at high annealing temperature would affected its specific surface area and catalytic performance[14].

Catalytic performance of lignin-derived NC for 4-NP reduction. After elucidation of structural characterization, the catalytic performance of N_{14}C-1373 was evaluated by 4-NP reduction to 4-AP with an excess $NaBH_4$ in water. Interestingly, $NaBH_4$ can not reduce 4-NP to 4-AP even after 3 h because of no observation of absorbance change determined by UV–Vis spectroscopy (Fig. 5a). However, the 4-NP solution color changes from light yellow to bright yellow with an absorbance at 400 nm after immediate addition of freshly prepared $NaBH_4$ solution. It is ascribed to the formation of 4-nitrophenolate ions in alkaline condition[40]. Moreover, a lot of bubble are observed to release from 4-NP solution. It is the consequence of hydrogen gas generated by hydrolysis reaction of $NaBH_4$[41]. Gratefully, when adding N_{14}C-1373 catalyst, the color of the reaction mixture is immediately changed from yellow to complete colorless within 50 s, indicating 4-NP is reduced to produce 4-AP (Fig. 5b). UV–vis spectroscopy demonstrates that the absorption band of 4-nitrophenolate ion

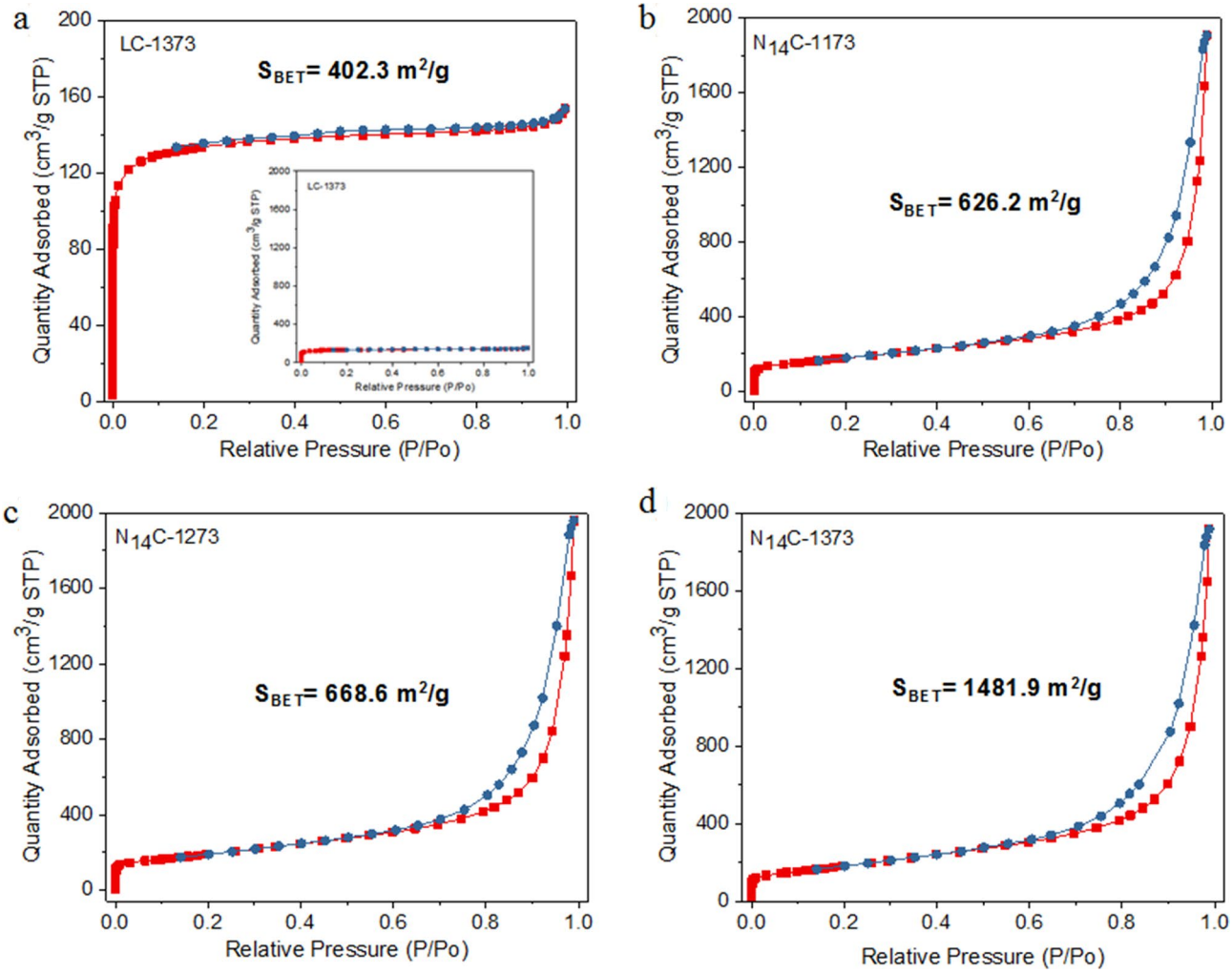

Figure 4. Effect of annealing temperature on BET surface area measurement of LC-1373 (**a**), $N_{14}C$-1173 (**b**), $N_{14}C$-1273 (**c**) and $N_{14}C$-1373 (**d**).

is at 400 nm, while the signal of 4-aminophenolate ion is at ~ 300 nm[19–21]. In Fig. 5b, two isosbestic points are also found at ~ 274 and 315 nm, a symbol of the complete conversion of 4-NP to 4-AP without the generation of intermediate byproducts, which has been considerably confirmed in the literature[23,39]. It is worthily noting that 4-NP reduction initiates immediately by adding $N_{14}C$-1373, and no induction time is required. This will be an outstanding clue for $N_{14}C$-1373 use in real technologies applications.

As seen from Fig. 5c,d, both g-C_3N_4/lignin ratio and annealing temperature have significant effects on the reaction kinetics parameters of N_xC-T catalysts, the apparent rate constants (k_{app}) and specific mass activity. It is interesting to note that the $N_{14}C$-1373 with the lowest total N content (3.3 atom %) shows the highest values of k_{app} (4.77 min^{-1}) and specific mass activity (361 mol kg^{-1} h^{-1}), probably due to the highest graphite N content (69.4%) and S_{BET} (1481.9 m^2/g). It is speculated that graphite N species and S_{BET} of NC plays a critical role for impelling 4-NP reduction rather than the total N atoms content[19–21]. Apple-to-apple comparisons of catalytic activities of $N_{14}C$-1173, $N_{14}C$-1273 and $N_{14}C$-1373, it is found that $N_{14}C$-1173 ($I_D/I_G = 1.03$) with the largest content of defective sites shows lower performance activity than $N_{14}C$-1273 ($I_D/I_G = 1.00$) and $N_{14}C$-1373 ($I_D/I_G = 0.97$), revealing that the catalytic activity of NC is not caused by the defect sites on the surface of catalysts, which is different from the results reported in the literature[31]. This contradictory phenomenon indicates that the effect of defect sites in NC on the catalytic performance needs further investigation in future.

The reaction kinetics of twenty catalysts prepared at different g-C_3N_4/lignin ratio and annealing temperature were conducted for 4-NP reduction, the kinetics experimental data were expressed by $\frac{C_t}{C_0} \rightarrow t$ (Fig. 6a,c,e,g). The assumption of pseudo-first-order kinetics is supported by the data of the linear fit between ln [C_t/C_0] and reaction time (t) (Fig. 6b,d,f,h) in the presence of a large molar excess of $NaBH_4$. The reaction following pseudo-first-order kinetics is different from N-doped graphene oxide[19,23], while it is similar to metallic catalysts[22,24–26]. Typically, the catalytic reduction of 4-NP over metallic catalysts is ascribed to a pseudo-first-order reaction[22,24–26]. N-doped graphene leads to the pseudo-zero-order reaction due to the limited number of active sites[19,23]. As described afored, N-doping species rather than the total N content will influence the catalytic performance of NC catalysts[19,23].

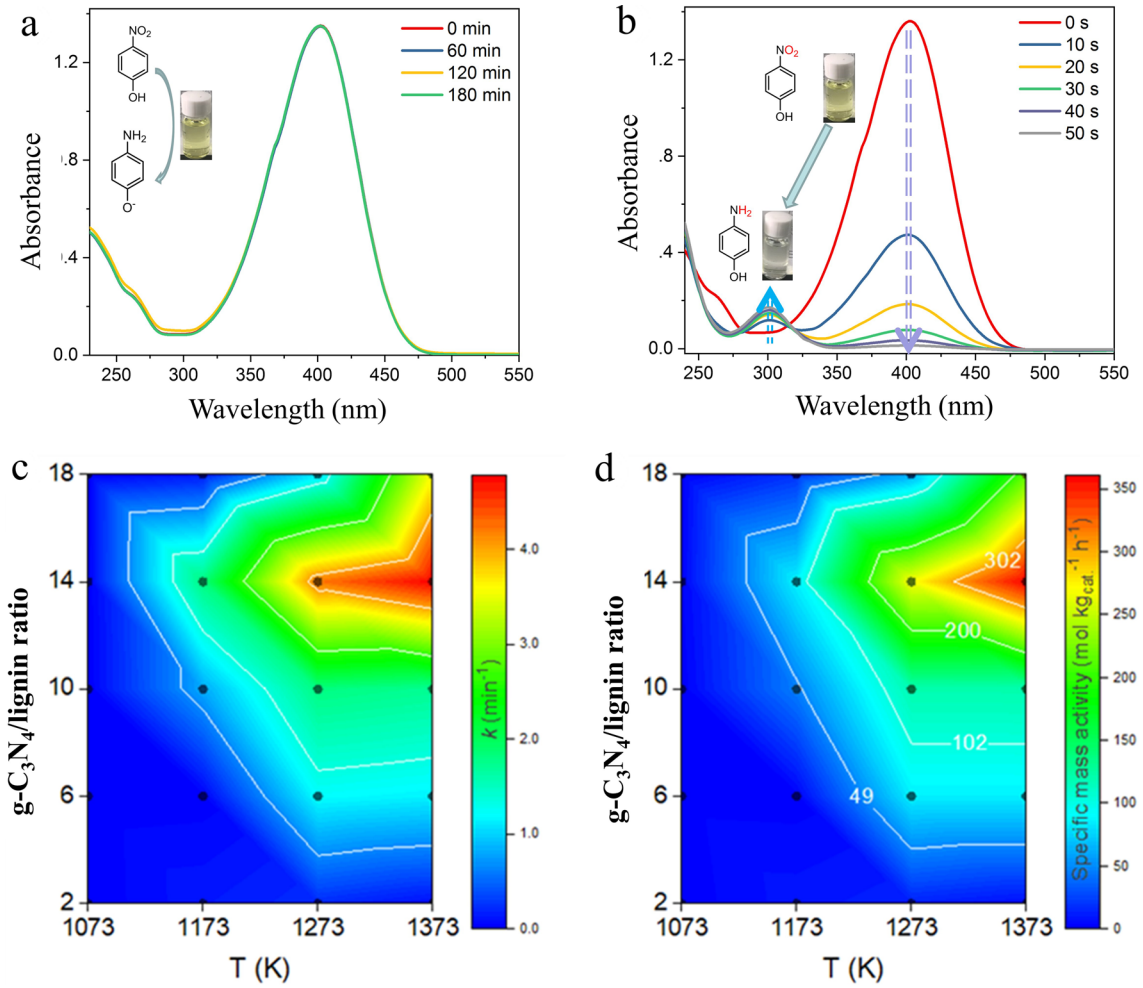

Figure 5. Catalytic performance of 4-NP reduction over lignin-derived NC catalyst. (**a**) Time-dependent UV–Vis spectra for the reduction of 4-NP with $NaBH_4$ in the absence of catalyst; (**b**) time-dependent UV–Vis spectra for the reduction of 4-NP by $NaBH_4$ in the presence of N_{14}C-1373. (**c**) Effect of annealing temperature and g-C_3N_4/lignin ratio on k_{app} value. (**d**) Effect of annealing temperature and g-C_3N_4/lignin ratio on specific mass activity.

To further insight into the effect of nitrogen dopant on the activity of lignin-derived NC catalysts, several counterparts including LC-1373, graphite powder, g-C_3N_4, graphene oxide (GO), and N_{14}C-1373 were compared for the conversion of 4-NP to 4-AP (Fig. 7a). In the absence of N-dopant, LC-1373, graphite and GO show little catalytic activity. It is also true for neat g-C_3N_4. These results strongly confirm that carbon atom without N-dopant and neat g-C_3N_4 have little contribute to 4-NP reduction reaction (Fig. 7a; Supplementary Table S3). That is to say, N-dopant plays a critical role in 4-NP reduction reaction over the as-synthesized NC catalyst[19,23]. NC as metal-free catalyst can avoid this problem and does not suffer from secondary contamination caused by metallic catalyst, even for commercial metallic Pb/C catalyst, due to metal leaching (Fig. 7b), From the linear relationshp of $\ln(\frac{C_t}{C_0}) \rightarrow t$ sinet of Fig. 7b, metallic Pb/C catalyst shows pseudo-first-order kinetics reaction with K_{app} value of 0.084 min^{-1}, far lower than N_{14}C-1373 (k_{app} = 4.77 min^{-1}) in our work. As summarized in Fig. 7c and Supplementary Table S4, the as-prepared N_{14}C-1373 shows the highest performance activity in the 4-NP reduction, and greatly outperforms most previously reported catalysts in the literature, regards of metallic and metal-free catalysts. Although N_{14}C-1373 shows excellent activity, however, the operational stability of the catalyst is equally vital to its activity. Thus, we investigated the durability of N_{14}C-1373 by recycling the catalyst and measuring its activity. Impressively, N_{14}C-1373 is highly reusable after six cycles without any loss of activity (Fig. 7d), revealing its outstanding stability and potential practical application in the coming years.

DFT calculation of 4-NP reduction over N_{14}C-1373. To address the catalytic mechanism of N_{14}C-1373 for 4-NP reduction, it was investigated the effect nitrogen dopants on the electronic structure of N_{14}C-1373 through DFT calculation. From the Bader charge and difference of charge in Fig. 8, the doped N atoms can introduce local high positive charge density and high spin density to their adjacent carbon atoms on the N_{14}C-1373 surface, leading to the carbon atoms activation with positive charges, which confers the carbon a metal-like d band electronic structure, and thus, a metal-like catalytic performance[18], its reaction kinetics can be described by the Langmuir isotherm[23]. Incorporation of the nitrogen dopants species will induce the charge redistribution

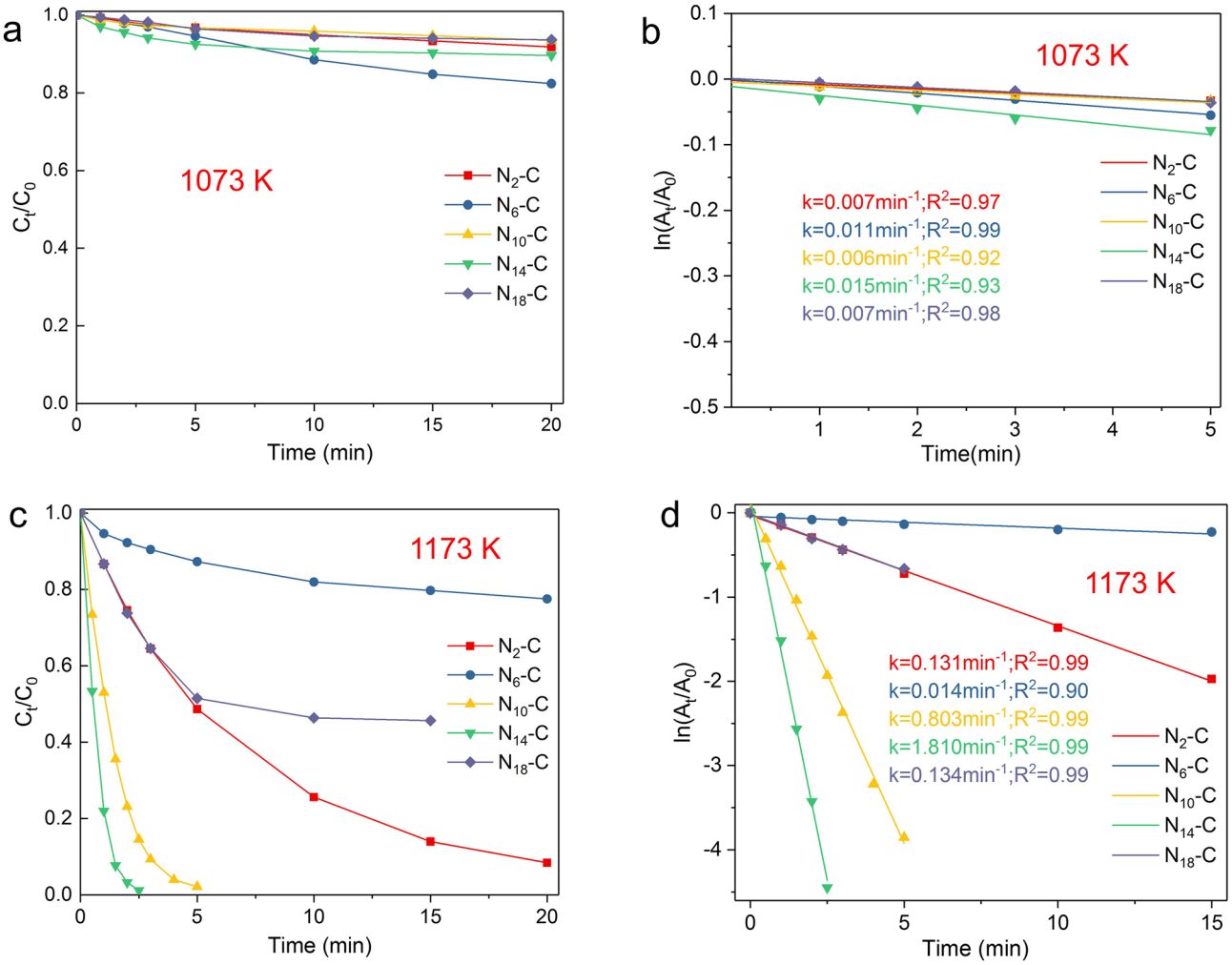

Figure 6. The reaction kinetics of the as-prepared NC catalysts at different g-C_3N_4/lignin ratio and annealing temperature for 4-NP reduction. The kinetic apparent rate constant (k_{app}) was calculated by using pseudo-first order kinetic model ($-k_{app}t = \ln \frac{C_t}{C_0}$). The experimental data of C_t/C_0 versus t are shown in (**a**,**c**,**e**,**g**) (left). The fitting plot curves of ln (C_t/C_0) versus t are shown in (**b**,**d**,**f**,**h**) (right).

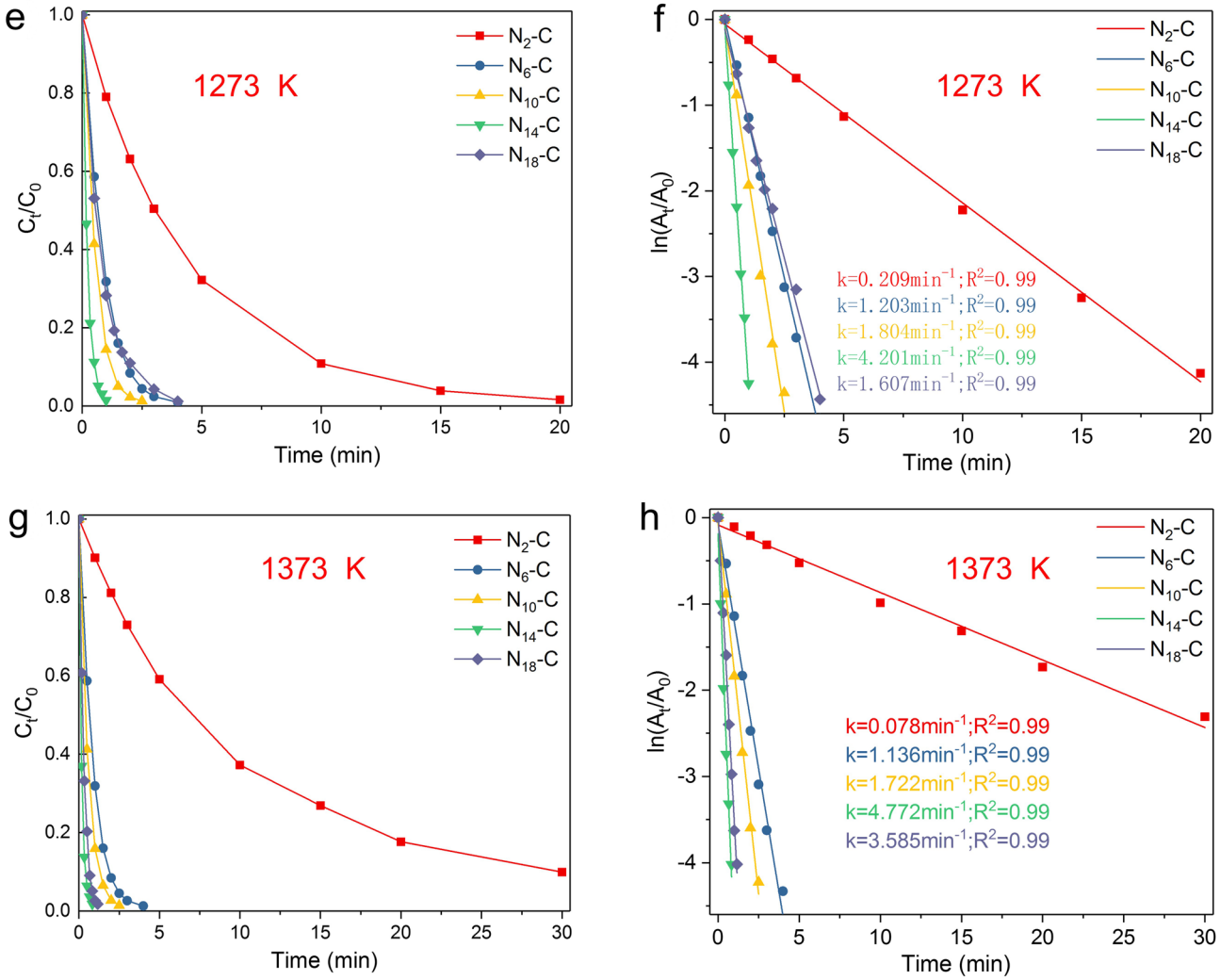

Figure 6. (continued)

and make the adjacent carbon bear a different positive charge (Fig. 8a). The greater of the number value in Fig. 8a is, the higher positive charge will be. For the difference of charge of graphitic, pyridinic and pyrrolic N in Fig. 8b, charge accumulates in N–C bonds. While for oxidized N species, apart form N–C bonds of charge accumulation, some charge is accumulating in oxygen atom.

Subsequently, the precise adsorption model of 4-NP over N_{14}C-1373 was proposed, and the contribution of the doped N species to catalytic performance was also evaluated using DFT. The optimized N_{14}C-1373 model is shown in Supplementary Fig. S3. Since the carbon active site on N_{14}C-1373 is positively charged due to the large electron negativity of the doped N atoms, the O atom of 4-NP is the preferred binding site[19,23]. Because 4-NP ion has two binding sites, nitro group and the O atom of hydroxyl substituents, it is further investigated the adsorption bond length and free energies of 4-NP ion over N_{14}C-1373 via nitro group and the O atom of hydroxyl substitutes, respectively. From the adsorption energies data in Supplementary Table S5, regardless of nitro group and the O atom of hydroxyl substituents binding sites, 4-NP adsorption reaction is spontaneous due to the negative adsorption energies. It indicates the 4-NP reduction reaction is too fast to detect the intermediate products. This explains the fact of the complete conversion of 4-NP to 4-AP without the generation of byproducts (Fig. 5b). From the view point of bond length and adsorption energies (Fig. 9; Supplementary Table S5), a meaningful conclusion has been drawn that four kinds of N dopants can improve the 4-NP adsorption ability of N_{14}C-1373 with different contribute to the catalytic properties. If the O atom of hydroxyl subtituents is the binding site, the graphitic N dopant species show the highest significant contribution to the catalytic activity due to its lowest adsorption free energy ($\Delta E = -3.6470$) and shortest adsorption bonding length (1.462 Å). On the contrary, considering nitro group as binding site, the oxidized N species exhibits the highest significant contribution to the catalytic activity due to its lowest adsorption free energy ($\Delta E = -0.8261$) and shortest adsorption bonding length (1.426 Å).

Basd on experimental data and DFT calculation, a plausible catalytic mechanism for 4-NP reduction over N_{14}C-1373 has been proposed and shown in Fig. 10. In the first step, hydrogen atom releasing from the adsorbed BH_4 was adsorbed on the surface of N_{14}C-137, simultaneously, 4-nitrophenolate ions are also absorbed on the carbon atoms active sites via nitro groups, which are activated for subsequent reduction. In the second step,

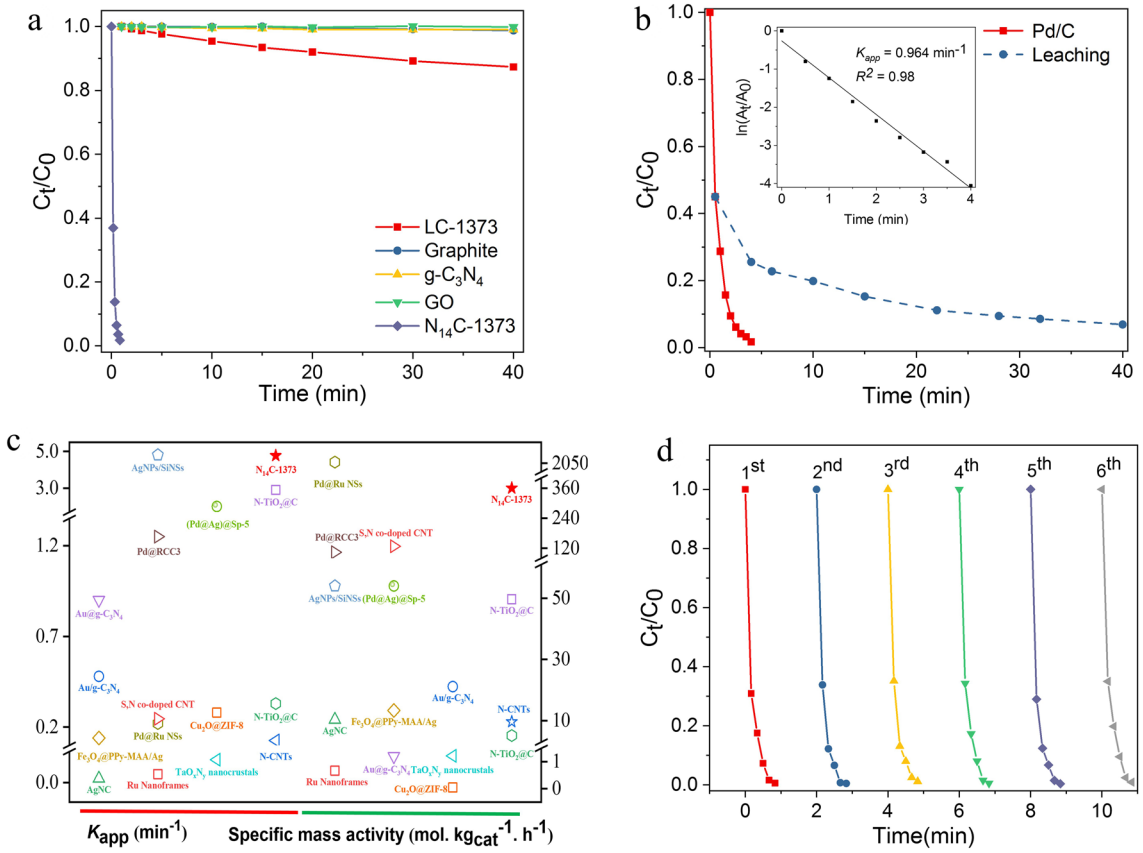

Figure 7. Activities comparison and stability of the as-prepared N_{14}C-1373. (**a**) Performance comparison of several counterparts catalysts. (**b**) Catalytic performance of commercial Pb/C catalyst. (**c**) Kinetics parameters comparison of N_{14}C-1373 with other catalysts reported in the literature. (**d**) Re-usability of N_{14}C-1373 after 6 runs.

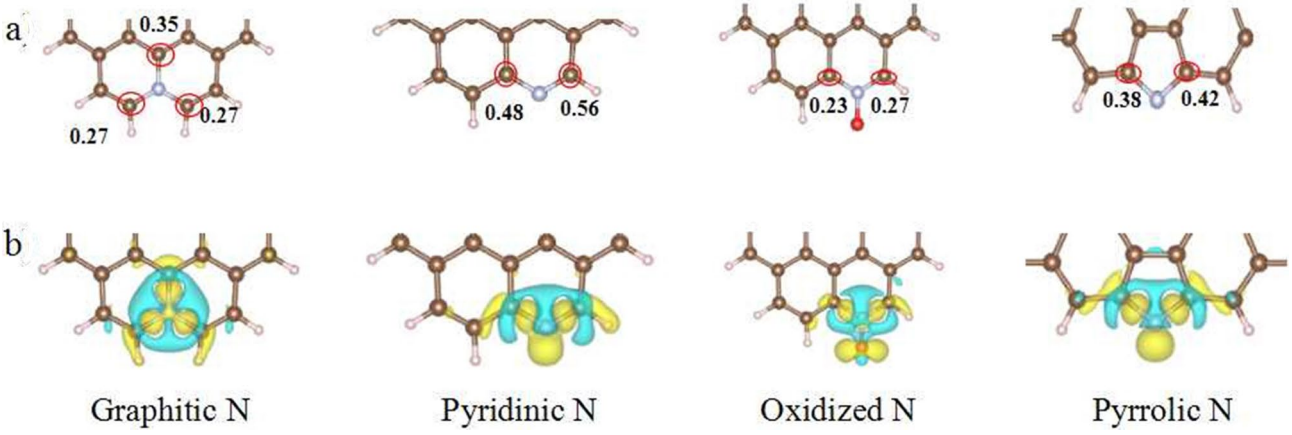

Figure 8. Bader charge and difference of charge of the as-prepared NC. (**a**) Bader charge, the digital number means the positive charge of carbon; (**b**) difference of charge. Yellow color represents charge accumulation, blue color indicates charge loss.

4-nitrophenolate ions are reduced by surface hydrogen species into the 4-aminophenolate ions intermediates. Then, 4-aminophenolate ions are absorbed on the carbon atoms active sites via the O atom of hydroxyl substituents. In the fourth step, 4-aminophenolate ions are reduced by surface hydrogen species into neutral 4-AP, which will desorption from the surface of N_{14}C-1373 surface and it creates a free surface for the next catalytic cycle. Therefore, the adsorption of 4-nitrophenolate ions is very critical for 4-NP reduction over N_{14}C-1373. A similar mechanism of 4-NP reduction has been found for metallic catalysts and N-doped graphite in the literature[22–26]. It is worthily noticed that the as-prepared N_{14}C-1373 has metallic properties with ample active sites, and the rates

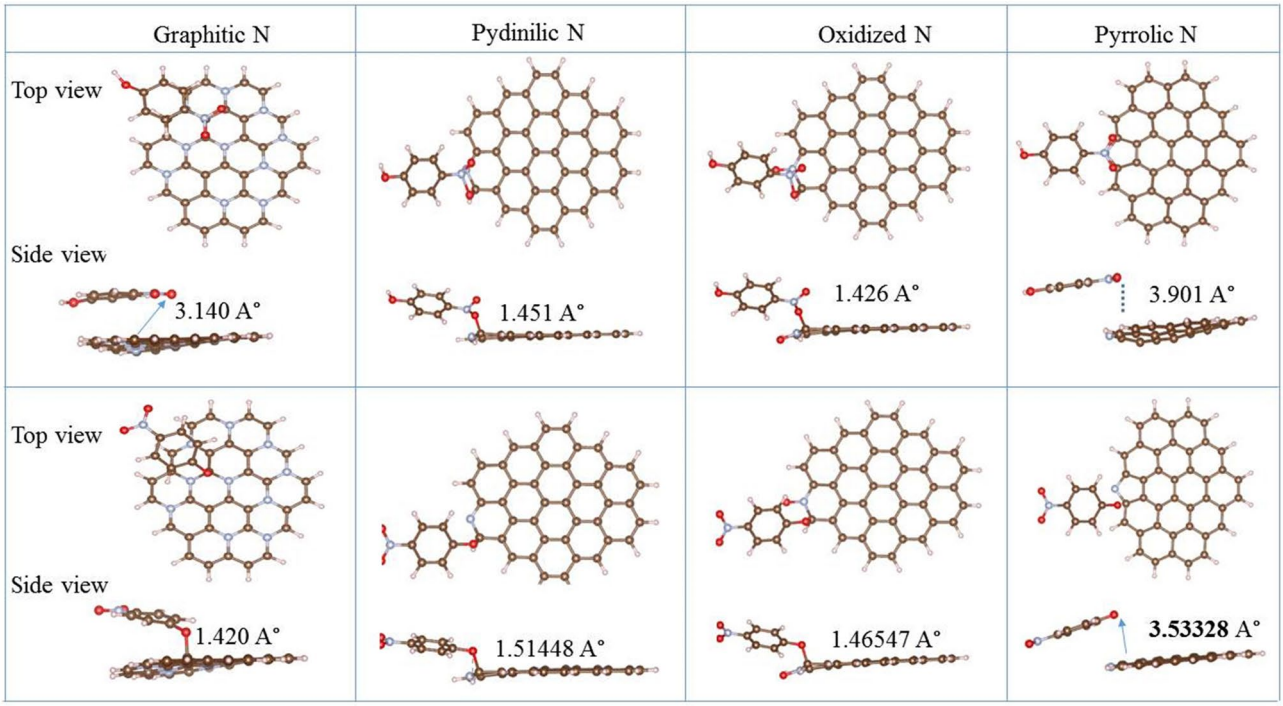

Figure 9. The optimized structures of 4-NP ions adsorbed on $N_{14}C$-1373: on the top line is nitro-group binding with graphitic, pyridinic, oxidized and pyrrolic N species; and the bottom line stands O atom in hydroxyl group binding with (graphitic, pyridinic, oxidized and pyrrolic N species. The separated distances for each model have been marked directly in the corresponding figures.

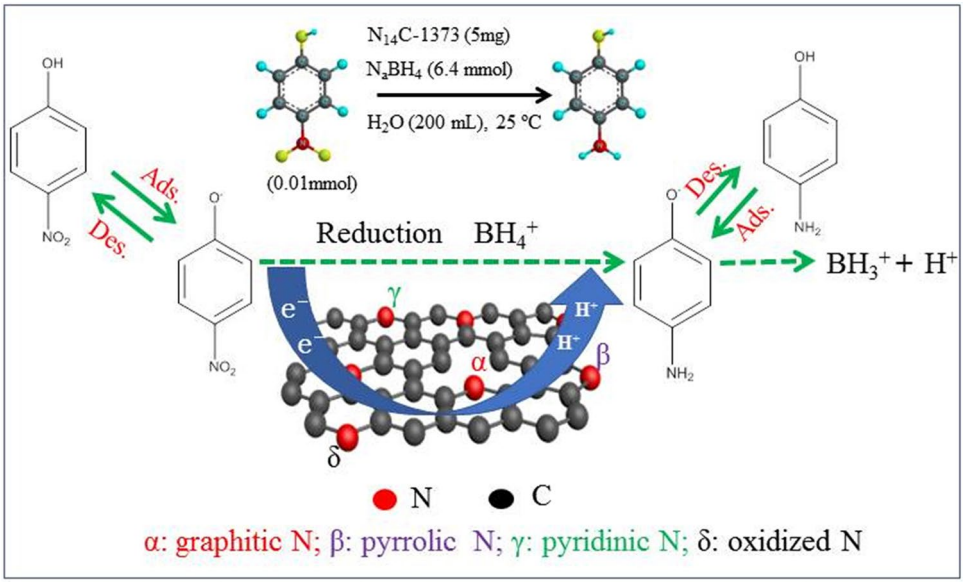

Figure 10. Possible catalytic mechanism of 4-NP reduction over lignin-derived $N_{14}C$-1373 using $NaBH_4$ as hydrogen donor in water at room temperature.

of substrate adsorption and product desorption are quite fast. Thus, the reduction kinetics is of pseudo-first-kinetics reaction, which can be described by the Langmuir isotherm[20,21]. In addition, the defect-rich structure of $N_{14}C$-1373 surface is not helpful to electronic transferring[42], which leads to low activity of catalyst. In contrast, the high BET surface area of catalyst results in strong adsorption ability and high-efficient electronic transferring, which can improve catalytic activity. In addition, $N_{14}C$-1373 with high concentration (69 at%) of graphitic N exhibits high electronic transfer activity for hydrogenation reaction[43]. These phenomena are in good agreement with the experimental data in Fig. 5c,d.

Conclusions

In summary, lignin-derived NC as metal-free catalyst has been successfully synthesized using lignin as carbon source and g-C_3N_4 as sacrificial template under different g-C_3N_4/lignin ratio and annealing temperature conditions. These NCcatalysts are evaluated for the catalytic reduction of 4-NP to 4-AP via hydrogen transfer in $NaBH_4$ aqueous system. Characterization detailed information shows that the as-prepared N_{14}C-1373 has the highest S_{BET} (1481.9 m^2/g) and graphitic nitrogen (69 at%). Kinetics investigation of 4-NP reduction over N_{14}C-1373 shows that it follows first-order reaction kinetics with $k_{app} = 4.77$ min^{-1} and specific mass activity (s = 361 mol. kg_{cat}^{-1} h^{-1}), which are the best values to date for 4-NP reduction. 4-NP ions adsorption has an essential influence on catalytic reduction, which initials spontaneously in the presence of N_{14}C-1373 catalyst. The charge density and adsorption models from DFT calculations demonstrate that the active sites of N_{14}C-1373 for 4-NP reduction are the carbon atoms adjacent to the N dopants, which contribute to catalytic performance in dependence of N dopants species, among which graphitic N species has much greater contribution to 4-NP adsorption. Because the nitrogen dopants can change the electronic structure of the adjacent carbon atoms and promote the chemical activity, DFT calculations verify that 4-NP ions will combine with active sites on N_{14}C-1373 surface via both nitro group and the O atom of hydroxyl group on the condition of low graphitic N species content. Interestingly, the as-prepared N_{14}C-1373 has excellent stability and good re-usability, as well as minimal contamination issues in comparison with commercial Pb/C catalyst.

Received: 25 April 2020; Accepted: 8 October 2020
Published online: 18 November 2020

References

1. Shuai, L. *et al.* Formaldehyde stabilization facilitates lignin monomer production during biomass depolymerization. *Science* **354**, 329–334 (2016).
2. Becker, J. & Wittmann, C. A field of dreams: Lignin valorization into chemicals, materials, fuels, and health-care products. *Biotechnol. Adv.* **37**, 107360 (2019).
3. Renders, T., Van den Bosch, S., Koelewijn, S. F., Schutyser, W. & Sels, B. F. Lignin-first biomass fractionation: The advent of active stabilisation strategies. *Energy Environ. Sci.* **10**, 1551–1557 (2019).
4. Ren, T., Qi, W., Su, R. & He, Z. Promising techniques for depolymerization of lignin into value-added chemicals. *ChemCatChem* **11**, 639–654 (2019).
5. Das, A. *et al.* Lignin conversion to low-molecular-weight aromatics via an aerobic oxidation-hydrolysis sequence: Comparison of different lignin sources. *ACS Sustain. Chem. Eng.* **6**, 3367–3374 (2018).
6. Hernandez, E. M. *et al.* Techno-economic and greenhouse gas analyses of lignin valorization to eugenol and phenolic products in integrated ethanol biorefineries. *Biofuels Bioprod. Bioref.* **13**, 978–993 (2019).
7. Rahimi, A., Ulbrich, A. J., Coon, J. & Stahl, S. S. Formic-acid-induced depolymerization of oxidized lignin to aromatics. *Nature* **515**, 249–252 (2014).
8. Wu, X. J. *et al.* Solar energy-driven lignin-first approach to full utilization of lignocellulosic biomass under mild conditions. *Nat. Catal.* **1**, 772–780 (2018).
9. Zhu, Y., Li, Z. & Chen, J. Applications of lignin-derived catalysts for green synthesis. *Green Energ. Environ.* **4**, 210–244 (2019).
10. Zhou, H., Xu, H. H. & Liu, Y. Aerobic oxidation of 5-hydroxymethylfurfural to 2,5-furandicarboxylic acid using Co/Mn-lignin coordination complexes-derived catalysts. *Appl. Catal. B-Environ.* **244**, 965–973 (2019).
11. Zhou, H. *et al.* Toward biomass-based single-atom catalysts and plastics: Highly active single-atom Co on N-doped carbon for oxidative esterification of primary alcohols. *Appl. Catal. B-Environ.* **256**, 117767 (2019).
12. Ren, X. H. *et al.* Synergic mechanism of adsorption and metal-free catalysis for phenol degradation by N-doped graphene aerogel. *Chemosphere* **191**, 389–399 (2018).
13. Su, D. S., Perathoner, S. & Centi, G. Nanocarbons for the development of advanced catalysts. *Chem. Rev.* **113**, 5782–5816 (2013).
14. Hu, H. W., Xin, J. H., Hu, H. & Wang, X. W. Structural and mechanistic understanding of an active and durable graphene carbocatalyst for reduction of 4-nitrophenol at room temperature. *Nano Res.* **8**, 3992–4006 (2015).
15. Hu, H. W., Xin, J. H., Hu, H., Wang, X. W. & Kong, Y. Metal-free graphene-based catalyst-insight into the catalytic activity: A short review. *Appl. Catal. A-Gen.* **492**, 1–9. https://doi.org/10.1016/j.apcata.2014.11.041 (2015).
16. Yu, H. *et al.* Nitrogen-doped porous carbon nanosheets templated from g-C3N4 as metal-free electrocatalysts for effificient oxygen reduction reaction. *Adv. Mater.* **28**, 5080–5086 (2016).
17. Zheng, L. *et al.* Ammonium nitrate-assisted synthesis of nitrogen/sulfur-codoped hierarchically porous carbons derived from ginkgo leaf for supercapacitors. *ACS Omega* **4**, 5904–5914 (2019).
18. Gao, Y. *et al.* Nitrogen-doped sp2-hybridized carbon as a superior catalyst for selective oxidation. *Angew. Chem. Int. Ed.* **52**, 2109–2113 (2013).
19. Yang, F., Chi, C., Wang, C., Wang, Y. & Li, Y. High graphite N content in nitrogen-doped graphene as an efficient metal-free catalyst for reduction of nitroarenes in water. *Green Chem.* **18**, 4254–4262 (2016).
20. Lin, Y. *et al.* Efficient and highly selective boron-doped carbon materials-catalyzed reduction of nitroarenes. *Chem, Commun.* **51**, 13086–13089 (2015).
21. Duan, Y., Song, T., Dong, X. & Yang, Y. Enhanced catalytic performance of cobalt nanoparticles coated with a N, P-codoped carbon shell derived from biomass for transfer hydrogenation of functionalized nitroarenes. *Green Chem.* **20**, 2821–2828 (2018).
22. Nguyena, T., Huang, C. P. & Doong, R. A. Enhanced catalytic reduction of nitrophenols by sodium borohydride over highly recyclable Au@graphitic carbon nitride nanocomposites. *Appl. Catal. B-Environ.* **240**, 337–347 (2019).
23. Kong, X., Sun, Z., Chen, M., Chen, C. & Chen, Q. Metal-free catalytic reduction of 4-nitrophenol to 4-aminophenol by N-doped graphene. *Energy Environ. Sci.* **6**, 3260–3266 (2013).
24. Islam, M. T. *et al.* Fullerene stabilized gold nanoparticles supported on titanium dioxide for enhanced photocatalytic degradation of methyl orange and catalytic reduction of 4-nitrophenol. *J. Environ. Chem. Eng.* **6**, 3827–3836 (2018).
25. Ye, W. *et al.* Green synthesis of Pt–Au dendrimer-like nanoparticles supported on polydopamine-functionalized graphene and their high performance toward 4-nitrophenol reduction. *Appl. Catal. B-Environ.* **181**, 371–378 (2016).
26. Wang, X., Liu, D., Song, S. & Zhang, H. Pt@CeO_2 multicore@shell self-assembled nanospheres: Clean synthesis, structure optimization, and catalytic applications. *J. Am. Chem. Soc.* **135**, 15864–15872 (2013).
27. Gazi, S. & Ananthakrishnan, R. Metal-free-photocatalytic reduction of 4-nitrophenol by resin-supported dye under the visible irradiation. *Appl. Catal. B-Environ.* **105**, 317–325 (2011).

28. Wang, S. *et al.* Layered g-C_3N_4@reduced graphene oxide composites as anodes with improved rate performance for lithium-ion batteries. *ACS Appl. Mater. Int.* **10**, 30330–30336 (2018).
29. Snelders, J. *et al.* Biorefining of wheat straw using an acetic and formic acid based organosolv fractionation process. *Bioresour. Technol.* **156**, 275–282 (2014).
30. Zhou, H. *et al.* High biomass loadings of 40 wt% for efficient fractionation to meet biorefinery in solvent aqueous system without adding adscititious catalyst. *Green Chem.* **18**, 6108–6114 (2016).
31. Zhu, J., Xiao, P., Li, H. & Carabineiro, S. A. C. Graphitic carbon nitride: Synthesis, properties, and applications in catalysis. *ACS Appl. Mater. Int.* **6**, 16449–16465 (2014).
32. Giri, S., Das, R., van der Westhuyzen, C. & Maity, A. An efficient selective reduction of nitroarenes catalyzed by reusable silver-adsorbed waste nanocomposite. *Appl. Catal. B-Environ.* **209**, 669–678 (2017).
33. Liu, K., Wu, G. & Wang, G. Role of local carbon structure surrounding FeN4 sites in boosting the catalytic activity for oxygen reduction. *J. Phys. Chem. C* **121**, 11319–11324 (2017).
34. Jiao, Y., Zheng, Y., Davey, K. & Qiao, S. Z. Activity origin and catalyst design principles for electrocatalytic hydrogen evolution on heteroatom-doped graphene. *Nat. Energy* **1**, 16130–16138 (2016).
35. Jiao, Y., Zheng, Y., Jaroniec, M. & Qiao, S. Z. Origin of the electrocatalytic oxygen reduction activity of graphene-based catalysts: A roadmap to achieve the best performance. *J. Am. Chem. Soc.* **136**, 4394–4403 (2014).
36. Graglia, M., Pampel, J., Hantke, T., Fellinger, T. P. & Esposito, D. Nitro lignin-derived nitrogen-doped carbon as an efficient and sustainable electrocatalyst for oxygen reduction. *ACS Nano* **10**, 4364–4371 (2016).
37. Sui, Z. Y. *et al.* Nitrogen-doped graphene aerogels as efficient supercapacitor electrodes and gas adsorbents. *ACS Appl. Mater. Inter* **7**, 1431–1438 (2015).
38. Rajkumar, C., Veerakumar, P., Chen, S. M., Thirumalraj, B. & Lin, K. C. Ultrathin sulfur-doped graphitic carbon nitride nanosheets as metal-free catalyst for electrochemical sensing and catalytic removal of 4-nitrophenol. *ACS Sustain. Chem. Eng.* **612**, 16021–16031 (2018).
39. Li, X., Wang, X. & Antonietti, M. Mesoporous g-C_3N_4 nanorods as multifunctional supports of ultrafine metal nanoparticles: Hydrogen generation from water and reduction of nitrophenol with tandem catalysis in one step. *Chem. Sci.* **3**, 2170–2174 (2012).
40. Zhao, P., Feng, X., Huang, D., Yang, G. & Astruc, D. Basic concepts and recent advances in nitrophenol reduction by gold- and other transition metal nanoparticles. *Coordin. Chem. Rev.* **287**, 114–136 (2015).
41. Ciganda, R. *et al.* Gold nanoparticles as electron reservoir redox catalysts for 4-nitrophenol reduction: A strong stereo electronic ligand influence. *Chem. Commun.* **50**, 10126–10129 (2014).
42. Ruan, Q. *et al.* Key factors affecting photoelectrochemical performance of g-C3N4 polymer films. *Chem. Commun.* **55**, 7191–7194 (2019).
43. Błonski, P. *et al.* Doping with graphitic nitrogen triggers ferromagnetism in graphene. *J. Am. Chem. Soc.* **139**, 171–3180 (2017).

Acknowledgements

This study was financially funded by the National Natural Science Foundation of China (NSFC, 21476016; 21776009), the special project for the construction of innovative province in Hunan Province of China (2019NK2031-3), and Hubei University of Science and Technology (2019-20KZ05).

Author contributions

Y.L. conceived and supervised this project, wrote the draft manuscript. H.X. prepared investigation and methods. H.Y. finished the DFT calculation, H.Y. finished methods, and T.C. completed FT-IR of N_{14}C-1737 catalyst. All figures are drawn by Y.L. and H.X.

Competing interests

The authors declare no competing interests.

Additional information

Supplementary information is available for this paper at https://doi.org/10.1038/s41598-020-76039-9.

Correspondence and requests for materials should be addressed to Y.L.

Reprints and permissions information is available at www.nature.com/reprints.

Publisher's note Springer Nature remains neutral with regard to jurisdictional claims in published maps and institutional affiliations.